



## Original Research Paper

Tensile strength of cohesive powders <sup>☆</sup>Pablo García-Triñanes <sup>a,\*</sup>, Stefan Luding <sup>b</sup>, Hao Shi <sup>b</sup><sup>a</sup> Flow, Heat and Reaction Engineering Group, FHRENG, Chemical Engineering Division, School of Engineering, University of Greenwich, United Kingdom<sup>b</sup> Multi-scale Mechanics, TFE, ET, MESA+, University of Twente, 7500 AE Enschede, The Netherlands

## ARTICLE INFO

## Article history:

Received 9 July 2019

Accepted 12 August 2019

Available online 28 August 2019

## Keywords:

Limestone

Schulze ring shear tester

Brookfield powder flow tester

Tensile strength

Cohesion

Shear index

Warren Spring model

## ABSTRACT

Measurement and prediction of cohesive powder behaviour related to flowability, flooding or arching in silos is found to be very challenging. Previous round robin [52] attempts with ring shear testers did not furnish reliable data and have shown considerable degrees of scatter and uncertainty in key measurements. Thus studies to build a reliable experimental database using reference materials are needed in order to evaluate the repeatability and effectiveness of shear testers and the adopted procedures.

In this paper, we study the effect of particle size on the yield locus for different grades of limestone (calcium carbonate). We use the nonlinear Warren Spring equation to obtain the values of cohesion  $C$ , tensile strength  $T$ , and the shear index  $n$ . We recover linear ( $n = 1$ ) yield loci for  $d_{50} > 70 \mu\text{m}$  with respectively small  $C$  and  $T$ , with consistent, finite macroscopic friction  $C/T = 0.7$ . With particle size decreasing below  $70 \mu\text{m}$  the response becomes more and more cohesive and non-linear ( $1 < n < 2$ ).

Then we compare the values of the parameters  $C$ ,  $T$  and  $n$  obtained from two different shear testers (Schulze and Brookfield PFT). Both testers run at positive confining stresses (slightly different ranges) and give identical results for large fractions (weakly cohesive). For strongly cohesive samples, the PFT results are very similar to the ring shear tester, with slightly smaller values for  $T$ ,  $C$ , and  $n$ . Further experiments with a variety of cohesive powders are needed to confirm or rebut this systematic difference the two testers display for cohesive powders.

Finally, we compare the (extrapolated) values of  $T$  with a direct, transverse measurement running at negative stresses, using the Ajax tensile tester, and found a very good agreement, which validates the Warren Spring equation for negative stresses.

© 2019 The Society of Powder Technology Japan. Published by Elsevier B.V. and The Society of Powder Technology Japan. This is an open access article under the CC BY-NC-ND license (<http://creativecommons.org/licenses/by-nc-nd/4.0/>).

## 1. Introduction

Granular materials underpin the performance of a vast array of everyday products. They are omnipresent in our daily life and widely used in many industries such as food, pharmaceuticals, paints, agriculture, plastics, mining, 3D printing, batteries, cosmetics or personal care products. During storage, flow or transportation in powder processing industry, the material faces various stress conditions and deformation, due to compression or shear.

Quality control in manufacturing (production plant) as well as manipulating the form and functionality of these industrially vital materials (R&D lab) is essential for commercial success and relies on a sound understanding of their properties. Linking particle

properties to powder performance in the process plant is essential. A lack of this can cause serious difficulties in aspects associated with flow, storage or handling, leading to lower productivity and dramatically affecting the performance of solids processing units.

Modern processing and formulation requirements have also led to a multi-scale approach to understand the failure of powders by means of mapping the necessary information from the particle level or primary particles to particle clusters (mesoscale) and finally towards the bulk behaviour. To characterize a small particulate sample by e.g. element tests or particle analysis and subsequently predict the bulk behaviour on the unit operation or process scale is of immense value.

Fascinating granular phenomena are: *yielding*, when the shear loads become extremely large the material fails in shear; *jamming*, when a dense stream of particles flows through an orifice, and they clog or jam, i.e. stop flowing, [1–4]; *dilatancy*, when they experience a volume change if subjected to shear deformations [5–7]; *shear – band – localization* when dilatant granular materials are sheared continuously under uniform stresses and strains [8,9]; *history – dependence* including direct time-dependent consolidation

<sup>☆</sup> Open Access for this article was sponsored by the Society of Powder Technology, Japan, through the KAKENHI Grant Number 18HP2009/Grant-in-Aid for Publication of Scientific Research Results, Japan Society for the Promotion of Science, 2019.

\* Corresponding author.

E-mail addresses: [p.garciatriñanes@gre.ac.uk](mailto:p.garciatriñanes@gre.ac.uk) (P. García-Triñanes), [s.luding@utwente.nl](mailto:s.luding@utwente.nl) (S. Luding), [h.shi-1@utwente.nl](mailto:h.shi-1@utwente.nl) (H. Shi).

## Nomenclature

$\sigma_0$	isostatic tensile strength (Pa)	$\Psi$	roundness ([-])
$F_H$	adhesion force (N)	$\sigma$	pre-consolidation normal stress (Pa)
$d_s$	Sauter mean diameter (m)	$\tau$	shear stress (Pa)
$\epsilon_o$	void fraction of the bed of particles ([-])	$\sigma_n$	normal stress (Pa)
$\rho_p$	particle density (kg/m <sup>3</sup> )	$\sigma_{pre}$	pre-shear normal stress (Pa)
$\rho_0$	initial bulk density (kg/m <sup>3</sup> )	$C$	cohesion or cohesive strength (Pa)
$\rho_b$	bulk density (kg/m <sup>3</sup> )	$T$	tensile strength (Pa)
$w$	moisture content (%)	$n$	shear index
$d_{10}$	particle diameter where 10% of distribution is below this value ( $\mu\text{m}$ )	$\mu$	friction coefficient
$d_{50}$	particle median size where 50% of distribution is below this value ( $\mu\text{m}$ )	$\phi_i$	internal friction angle
$d_{90}$	particle diameter where 90% of distribution is below this value ( $\mu\text{m}$ )	$\sigma_C$	cohesive characteristic consolidation (Pa)
		$n_C$	cohesion index
		$\sigma_T$	tensile characteristic Consolidation (Pa)
		$n_T$	tensile strength index

effects and load history-dependent cohesion [10]; or *anisotropy* when sheared systems show direction-dependent distributions of both the contact network and the contact forces [11–13] have attracted significant scientific interest over the past decades [14–22].

The mechanical behavior of cohesive powders depends on pre-stressing history [23]. Various laboratory testers to study the shear stress necessary for the failure of consolidated powder beds can be found in the literature to evaluate the bulk behaviour of granular materials [24,25]. These testers are also a valuable tool to understand the influence of particle properties, e.g. density, size-distribution and shape, on the macroscopic bulk response. Moreover, such shear testers are commonly used for the industrial design of silos and hoppers. Although this is in many cases still empirical, the design methods are based on fundamental engineering principles and follow norms and established sample preparation procedures [26–29].

Element tests are (ideally homogeneous) macroscopic tests in which the force (stress) and/or displacement (strain) path are controlled. The most widely performed element test in both industry and academia is the shear test, where a granular sample is sheared until failure is reached and the material starts to flow.

Shear testers are usually classified into two groups: direct and indirect methods [25,27]. In direct shear testers, the shear zone is pre-defined by the device design, and the shear failure is forced in a specific physical location. On the contrary, in the indirect devices, the shear zone develops according to the applied state of stress. The most common indirect devices are the uni-axial compression tester [10,30,31] and the bi-axial shear box [32,33].

Direct devices can be further categorised into two sub-groups: translational and rotational. Typical translational shear testers include the direct shear tester [34–36] and the Jenike shear tester [37], while torsional or rotational shear testers include the FT4 powder rheometer [38], the Schulze ring shear tester [39] and the Brookfield powder flow tester [40].

A similar classification can be established attending to the movement of the shear cell elements and distinguishing between four main categories: the rotational cells, parallel plate cells and upper or lower movable shear cells. Detailed reviews of testers have been presented by several authors [25,41,42], and more (non-commercial) shear testers with higher complexity can be found in literature [43–45].

All shear testers have in common that they measure the shear stress necessary to make a sample yield under a given finite compressive normal stress.

On the other hand, the tensile strength can be defined as the tensile normal stress required to fracture a specimen of compacted

powder when no shear forces are applied. It represents the tendency of a sample of compacted powder to resist separation from a particle bed under the influence of a tensile stress and it is the external macroscopic manifestation of attractive forces between the constituent particles.

The magnitude of these forces depends on the closeness of particles in the packing, like the yield stress the tensile strength is related to the present state due to stress history of the particulate solid.

For cohesive powders, the tensile strength increases with increasing packing density due to the increase in the number and intensity of interparticle forces (adhesion, cohesion, van der Waals, interfacial, bridging and interlocking) [46–48].

The direction and module of compacting stresses must be defined in relation to the alignment of the plane in which failure takes place.

$C_o$  – axial tensile strength relates to failure stress in the direction opposite to the compacting stress. *Transverse* tensile strength relates to failure stress at 90° to the orientation of the compacting stress. *Ultimate* tensile strength is a measure of the failure stress of a triaxially compacted sample. (A theoretical, rather than a practical test). *Isostatic* tensile strength in the absence of deformation (unconsolidated particle contacts) represents the characteristic cohesive nature of a powder.

The isostatic tensile strength  $\sigma_0$  can be related to the adhesion force,  $F_H$  using the pioneer approach of Rumpf (1962) [49]:

$$\sigma_0 = \frac{(1 - \epsilon_o)F_H}{(\epsilon_o d_s^2)} \quad (1)$$

where  $d_s$  represents the mean Sauter diameter of the particles and  $\epsilon_o$  is the void fraction (porosity) of the bed of particles with  $(1 - \epsilon_o)/\epsilon_o$  being the inverse void ratio.<sup>1</sup> Capece (2015) [50] investigated the fundamental relationship between interparticle cohesion and powder flowability making use of the Bond number as a dimensionless quantification of the cohesion between particles. A model to study the effect of physical properties on cohesion and unconfined yield strength of pharmaceutical powders considering particle size and compressibility index was presented by Garg (2018) [51].

Quality and reproducibility of results are key aspects for proper material characterization. Although shear testing technologies have been developed and studied extensively, significant scatter in measurements is still common when testing powder flowability using different devices in different labs/environments [38–40,52–54].

<sup>1</sup> The inverse void ratio increases with decreasing the porosity and thus that increases the isostatic tensile strength.

Previous studies have been focusing on this problem by performing round-robin experimental studies on the Jenike tester [55], the Schulze ring shear tester [52] and the Brookfield powder flow tester [40] as well as comparing different devices [56,57].

The earliest round-robin study [55] resulted in a certified material (CRM-116 limestone powder) and a common standard experimental testing procedure for determining the yield locus. Schulze (2011) [52] has collected 60 yield loci obtained using the small Schulze shear tester RST-XS (21 labs) and 19 yield loci using the large Schulze shear tester RST-01 (10 labs) on one limestone powder (CRM-116). Results have been compared among them as well as with the results from a reference Jenike tester. While results from RST-01 and RST-XS are in good agreement, a considerable deviation (up to 20 %) was observed when comparing results from the Schulze ring shear tester to the Jenike shear tester.

Similar results are found by other researchers [40,56,58], where yield loci from the Brookfield powder flow tester, the Schulze ring shear tester, the FT4 powder rheometer and the Jenike shear tester are compared. The Brookfield powder flow tester and the FT4 powder rheometer show systematically lower shear resistance in comparison to the other two shear testers.

Other studies have compared different industrially relevant powders but only in a single device [59,60]. Moreover, these comparative studies have been limited to relatively low stresses. A deeper understanding of the reasons for the differences in measured flow behaviour of powders in several shear devices over a wide stress range is still missing and remains a huge challenge for the particle technology community.

This article aims to shed light on the measurement and the importance of the tensile strength of cohesive powders and it is structured as follows: In Section 2, we provide information on the limestone samples/materials, before we describe in Section 3, the experimental devices and the test procedures. Section 4 is devoted to the description of the Warren Spring model for tensile and cohesive strength and in Section 5 we discuss the experimental results with focus on the measurement of powder failure properties, while conclusions and outlook are presented in Section 6.

## 2. Material description and characterization

Limestone powder is widely used in many fields ranging from construction, toothpaste to automotive industries. Following previous work [24], we have chosen the same grades of pre-sieved limestone powders under the commercial name Eskal (KSL Staubtechnik GmbH, Germany). The limestone powder has been used as a reference material for standard testing [24,61,62] in powder technology due to the favourable physical properties: high roundness, low porosity and an almost negligible sensitivity towards humidity and temperature changes.

The raw Eskal granules (calcium carbonate of approx. 4 mm) are all ground passing a pin mill to reduce the particle size. Very fine particles are eliminated by a cyclone while the remaining particles

pass an air classifier and in the next step are sieved to different grades of particle size distributions. The details of their physical properties are summarized in Table 1.

As previous studies indicate a non-linear yield locus is correlated to the cohesiveness of the powder, the focus here is on the most cohesive grade of Eskal. While in [24], the focus was more on their low stress response, the current study reaches out to the behaviour of fine/cohesive Eskal300 ( $d_{50} = 2.22 \mu\text{m}$ ) and coarse/free-flowing Eskal150 ( $d_{50} = 138 \mu\text{m}$ ) at lower confining stress.

### 2.1. Measurements

The particle size data was obtained using laser diffraction in the dry method by means of a RODOS dispersion system with feeder VIBR/L (Sympatec GmbH). The measurements were performed under repeatability conditions.

Surface area measured by BET Automatic Specific Surface Analyzer Macsorb by MounTech Co., Ltd. The initial bulk density values are provided by the manufacturer. Particle density was measured using a Helium pycnometer (UltraPyc 1200e). Note that all powders here are presented with their original commercial name (e.g. Eskal150, Eskal300), while their median particle size  $d_{50}$  will be used for future discussions for the sake of clarity.

The aspect ratio, shape and morphology of all Eskal samples are analyzed by Scanning Electron Microscope (SEM) imaging (Helios G4 CX, FEI Deutschland GmbH, Germany). Figs. 1 and 2 show the SEM images of Eskal150 and Eskal300, respectively. In Fig. 1, we see that all the Eskal150 primary particles have similar shapes (left) and rough surfaces (right), and every particle can be clearly distinguished from the others. But for Eskal300 in Fig. 2 (left), we observe some clusters of primary particles, and the size of clusters are typically around 10–20  $\mu\text{m}$ , which is about 5–10 times the median particle size of Eskal300. When we zoom into smaller scale focusing on only one cluster as shown in Fig. 2 (right), we see even smaller fines (<1  $\mu\text{m}$ ) sticking on the surface of primary particles, and the shape of Eskal300 particles are slightly more irregular than the ones from Eskal150. The other Eskal samples are very similar in their shapes irrespective of median particle size, with roundness increasing with size, and specific surface area decreasing.

## 3. Experimental setup

### 3.1. Schulze ring shear tester - RST-01 and RST-XS

The Schulze ring shear tester (1994) is one of the most widely used testers in powder flowability characterization. The Schulze ring shear tester (RST-01) is connected to a computer with controlling software that allows the user to obtain semi-automatically the yield loci and wall yield loci. A smaller version of the ring shear tester with exactly the same working principle is the so-called RST-XS, developed for both smaller specimen volumes (3.5 ml to 70 ml, rather than 204 ml for the RST-01) and smaller confining/

**Table 1**  
Material parameters of the experimental samples with focus on the two samples in bold font.

Property	Eskal	Unit	300	500	15	30	80	150
Particle Size	$d_{10}$	$\mu\text{m}$	<b>0.78</b>	1.64	12	21	39	<b>97</b>
	$d_{50}$	$\mu\text{m}$	<b>2.22</b>	4.42	19	30	71	<b>138</b>
	$d_{90}$	$\mu\text{m}$	<b>4.15</b>	8.25	28	43	106	<b>194</b>
Span	$(d_{90}-d_{10})/d_{50}$	[-]	<b>1.52</b>	1.50	0.84	0.73	0.94	<b>0.70</b>
Particle density	$\rho_p$	$\text{kg}/\text{m}^3$	<b>2853</b>	2868	2799	2758	2753	<b>2761</b>
Moisture content	$w$	%	<b>0.9</b>	0.9	0.9	0.9	0.9	<b>0.9</b>
Roundness (sphericity)	$\Psi$	[-]	<b>0.75</b>	0.55	0.48	0.66	0.84	<b>0.88</b>
Initial bulk density	$\rho_0$	$\text{kg}/\text{m}^3$	<b>540</b>	730	1110	1230	1330	<b>1370</b>
Specific surface area	SSA	$\text{m}^2/\text{g}$	<b>2.324</b>	1.096	0.538	0.390	0.353	<b>0.310</b>

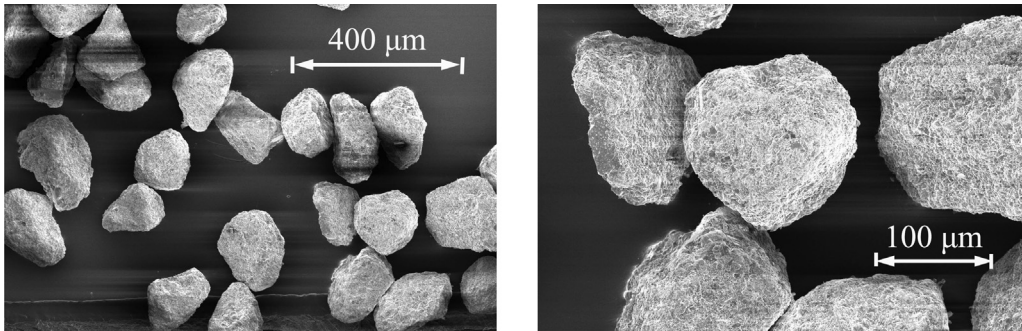


Fig. 1. SEM topography images of Eskal150 ( $d_{50} = 138 \mu\text{m}$ ) in two different scales: 400  $\mu\text{m}$  (left) and 100  $\mu\text{m}$  (right), as indicated by the scale bar.

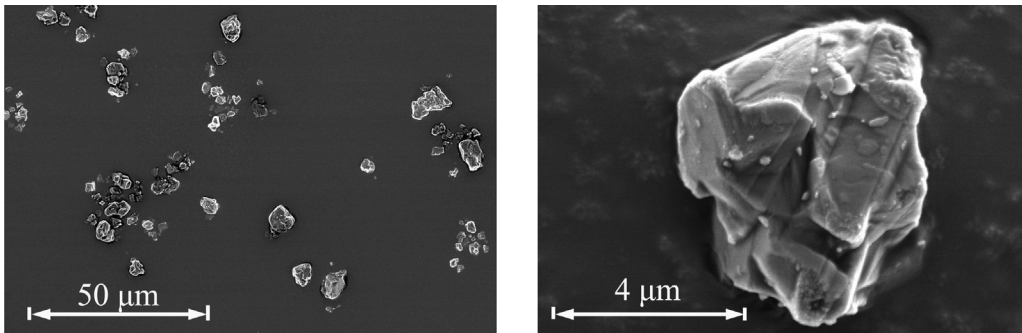


Fig. 2. SEM topography images of Eskal300 ( $d_{50} = 2.2 \mu\text{m}$ ) in two different scales: 30  $\mu\text{m}$  (left) and 4  $\mu\text{m}$  (right), as indicated by the scale bar.

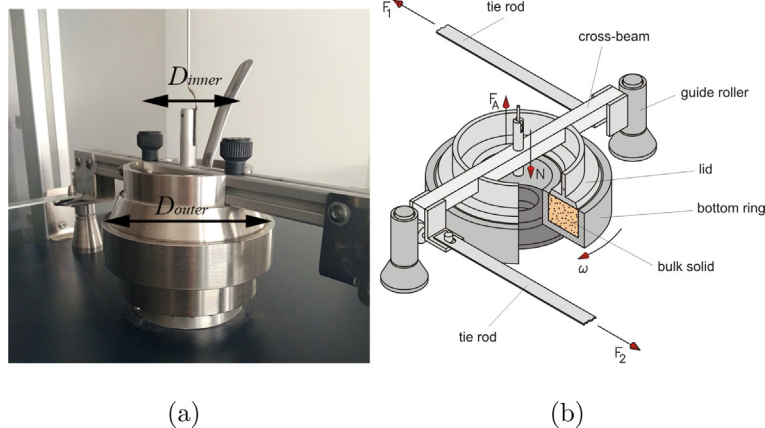


Fig. 3. (a) The Schulze ring shear tester RST-01 and (b) the working principle of the Ring shear cell set-up. The difference between RST-XS and RST-XS is the shear cell size. For technical details see Table 2. (b), reprinted with permission from author [63]. Copyright: Dietmar Schulze.

pre-consolidation stresses. For both versions of the shear tester, the bulk solid specimens are filled inside an annular bottom ring. An annular-shaped lid is then placed on top of the bulk solid specimen and is attached to a cross-beam (Fig. 3).

A normal force,  $F_N$ , is exerted on the cross-beam perpendicular to the rotational plane and transmits through the lid onto the specimen. In order to allow small confining stress, the counterbalance force,  $F_A$ , is introduced (see Table 2). It acts in the centre of the cross-beam, directed vertically upwards, counteracting the gravitational force of the lid, the hanger and the cross-beam. By rotating the bottom ring with an angular velocity  $\omega$  and keeping the cross-beam stationary with two tie-rods, the sample is sheared

effectively. Each of the tie-rods is fixed at a load beam, so that the forces,  $F_1$  and  $F_2$ , can be measured. The bottom of the shear cell and the lower side of the lid are rough in order to prevent sliding of the bulk solid on these two surfaces. Through this shearing the bulk solid is deformed, and a shear stress  $\tau$  develops, proportional to the forces acting on the tie-rods ( $F_1 + F_2$ ). In addition to the shear forces ( $F_1, F_2$ ), the ring shear tester also measures the vertical position of the lid. If a bulk solid is compressible, its bulk density,  $\rho_b$ , will increase with the normal load applied. Thus, also the volume of the bulk solid specimen can be deduced from the known vertical position of the lid. All the tests performed here follow the ASTM standard [64].

**Table 2**  
Specifications comparison of the Schulze ring shear tester RST-01 and RST-XS.

Property	RST-01	RST-XS
Cell volume (cm <sup>3</sup> )	204	31.4
Cell geometry	Ring	Ring
Wall material	Aluminium and PVC	Aluminium
Diameter ( <i>D</i> ) (cm)	6 (inner) 12 (outer)	3.2 (inner) 6.4 (outer)
Shear displacement limit (cm)	Unlimited	Unlimited
Test control	Computer	Computer
Sample weighing	Offline	Offline
Compression device	Top ring	Top ring
Driving velocity (°/min)	0.0038–22.9	0.0038–22.9
Max. normal stress (kPa)	50	20
Sample conditioning before pre-shear	Pluviation (manual)	Pluviation (manual)
Yield locus test duration	20 min	20 min
Stress measure direction	Rotational	Rotational

### 3.2. Brookfield powder flow tester – PFT

The Brookfield tester (Fig. 4) has been designed to minimise the operator involvement in the shear testing process [40]. The apparatus is computer controlled via a USB link to reproduce the sequences of normal stresses and the shear movement necessary to define the yield loci using the Powder Flow Pro software. It is possible to obtain in one single measurement: Unconfined failure strength, major principal consolidating stress, time consolidation, angle of internal friction, cohesion and bulk density.

The Brookfield Powder Flow Tester allows in a separate test to investigate the evolution of wall friction with increasing shear distances over the wall. This shear tester operates by applying a normal compression on to the powder sample sandwiched in the annular space between the trough and the vane lid. The standard

**Table 3**  
Specifications comparison of the Brookfield powder flow tester with normal and small cells.

Property	Normal cell	Small cell
Cell volume (cm <sup>3</sup> )	230	38
Vane lid (cm <sup>3</sup> )	33	5
Cell geometry	Ring	Ring
Wall material	Aluminium	Aluminium
Diameter ( <i>D</i> ) (cm)	15.24	12.70
Shear displacement limit (cm)	Unlimited	Unlimited
Test control	Computer	Computer
Sample weighing	Offline	Offline
Compression device	Top ring	Top ring
Driving velocity (cm/s)	0.01 to 0.5	0.01 to 0.5
Load for Vertical	7	7
Axis Compression (kg)		
Sample conditioning before pre-shear	Pluviation (manual)	Pluviation (manual)
Yield locus test duration	18 min	18 min
Stress measure direction	Rotational	Rotational
Trough rotational speed	1 revolution/hour (RPH) up to 5 RPH	1 revolution/hour (RPH) up to 5 RPH

vane lid has 18 small compartments which trap the powder particles and cause them to shear against the powder particles in the trough. When the standard trough is filled to level, it holds 230 cm<sup>3</sup> of sample material with an external annulus diameter of 15.24 cm (see Table 3). When used with the standard vane lid, the additional volume required for the lid increases to 263 cm<sup>3</sup> of material. The axial speed of the lid approach movement and rotational speed can be set by the user. The underside of the trough has recessed vanes or a perforated screen to grip the powder sample. A



**Fig. 4.** Brookfield powder flow tester highlighting the two different trough sizes. For technical details see Table 3. Copyright: Brookfield AMETEK. Develped in association with The Wolfson Centre for Bulk Solids Handling Technology, University of Greenwich, UK

small volume shear cell kit version of this tester with exactly the same working principle was developed for smaller specimen volumes. The small trough requires 38 cm<sup>3</sup> of sample when filled to level with an external annulus diameter of 2.7 cm. When used with the small vane lid, the total sample size increases to 43 cm<sup>3</sup>. Other important parts of the PFT are the inner and outer catch trays and the shaping blade to level the powder sample.

The powder sample is initially consolidated by continuously shearing it under the chosen compacting load and it is then sheared to failure under reduced normal loads. This process starts with the lowest load and is repeated with increasing normal loads until a complete locus can be plotted. Note that the Brookfield PFT operates over a lower normal stress range (0.3 to 5 kPa) than the RST although 13 kPa can be reached when using the small cell.

### 3.3. Tensile strength measurement

In this study the tensile strength,  $T$ , was directly obtained using a transverse tensile tester (Ajax Equipment Ltd) that uses uniaxial compaction followed by failure due to tension applied at 90° to the compacting stress. The tensile strength is equal to the external tensile force per area on the Eskal sample at failure when no shear force is applied. This tester is a refinement of the device developed by Warren Spring Laboratories. The device allows for direct measurement of the force required to fracture a sample of Eskal contained in a split cell (see Fig. 5). One half of the split cylindrical

cell is attached to the main body of the machine whilst the matching section is mounted on a leaf spring. Twin opposing action tension springs are each attached to screw adjusting blocks so that the moving cell can be positioned in a contact-null balance position against the fixed half. An amount of Eskal to just reach the required density for the test is filled in the loading cylinder and the top surface is carefully levelled. A plunger equivalent to a consolidating stress of 3 kPa is put onto the cylinder until the shoulder sits on top of the rim of the cell loading cylinder. Caution was taken not to tighten or rotate the plunger to avoid any degree of shear stress on the sample, which would cause anisotropy and too complex stresses. The plunger is then withdrawn and the loading cylinder removed. The out balance stress applied to the cell is then measured on the loading screw. The tensile strength is given by the extension and the value at tensile failure in conjunction with a calibration graph. A minimum of six tests were undertaken to ensure reliable results with good reproducibility.

### 4. Warren-spring model

The shape of the yield locus,  $\tau(\sigma_n)$ , the shear stress needed to cause failure at the applied normal stress,  $\sigma_n$ , can be approximated by the Warren Spring equation [46,47]:

$$\tau(\sigma_n) = C \left( \frac{\sigma_n}{T} + 1 \right)^{\frac{1}{n}} \tag{2}$$

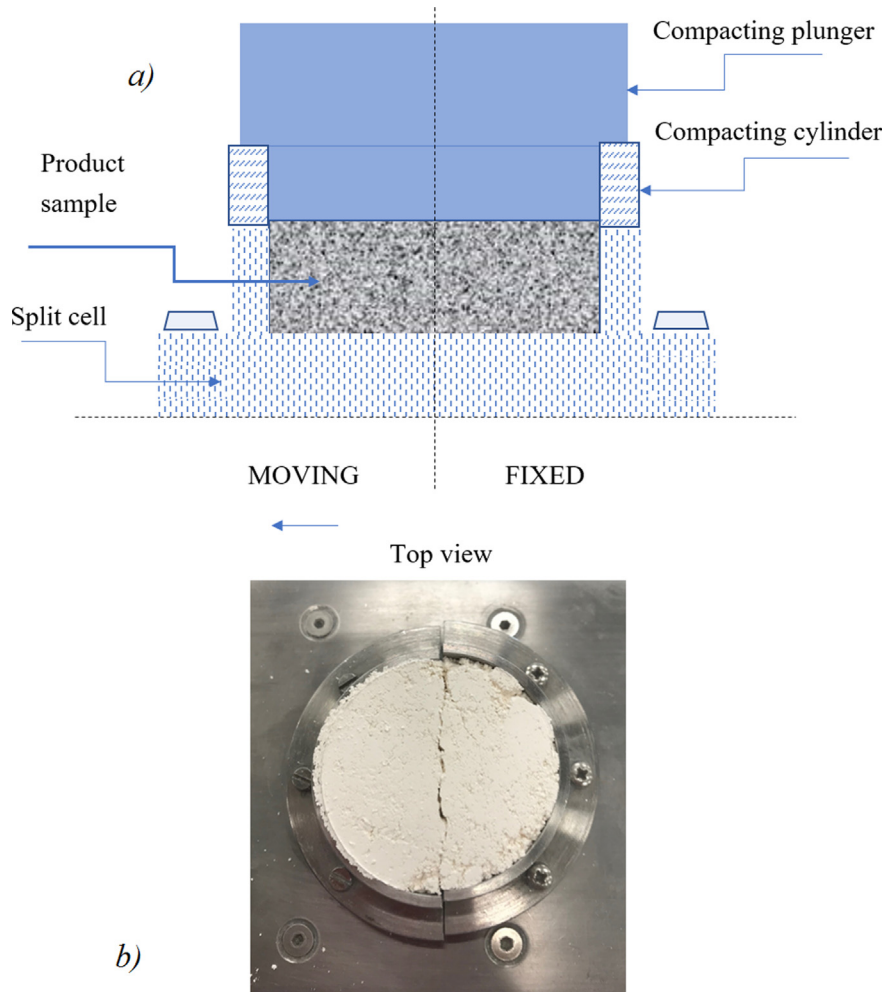


Fig. 5. (a) Ajax Equipment full volume cell illustrated. (b) Eskal300 sample springing apart.

which incorporates the tensile strength,  $T$ , the cohesion,  $C$ , and the exponent,  $n$ , named curvature or shear index, that takes values between 1 and 2.

The model agrees with the Coulomb Yield Criterion, if and only if, shear index equals 1 since then the friction coefficient  $\mu$  of the powder equals  $C/T$ .

$$\tau = C + \mu\sigma_n \quad (3)$$

where  $\mu = \tan\phi_i$  is related to the internal friction angle.

Previous authors [46,65] claimed that the parameter  $n$  characterizes the flowability of the powder sample but to date the micro-mechanical origin and the physical meaning of this parameter could not be explained. The extrapolation of a curved line through limited data with a high variation or uncertainty has generated controversy over the years and a number of researchers have proposed different empirical equations to describe the shapes of yield loci [66–68]. Here, we do not refer to the other models for the sake of brevity because Eq. (2) fits our data pretty well.

## 5. Results and discussion

In this section, we use different size limestone powders and we compare the measurement from different shear devices to give a general overview on the repeatability and reproducibility of the test results. In order to compare the yield loci from different testers, two limestone powders were chosen as reference powders for device comparison as described in Table 1: cohesive Eskal300 (2.22  $\mu\text{m}$ ) and free flowing Eskal150 (138  $\mu\text{m}$ ). The shear measurements with the Schulze ring shear tester and the Brookfield powder flow tester were conducted independently by the authors in two different countries.

Finally, we examine the quality of the Warren-Spring model by fitting the model on the raw data from both shear devices.

### 5.1. Yield Loci of Limestone powders using RST and PFT

As first step, we look at the raw yield loci of RST-01 using all the above mentioned materials as shown in Fig. 6.

We observe that the yield loci are almost linear when the median particle size is larger than 140  $\mu\text{m}$ , and this linear locus is not helpful on our main focus in this study, therefore, we decide to take

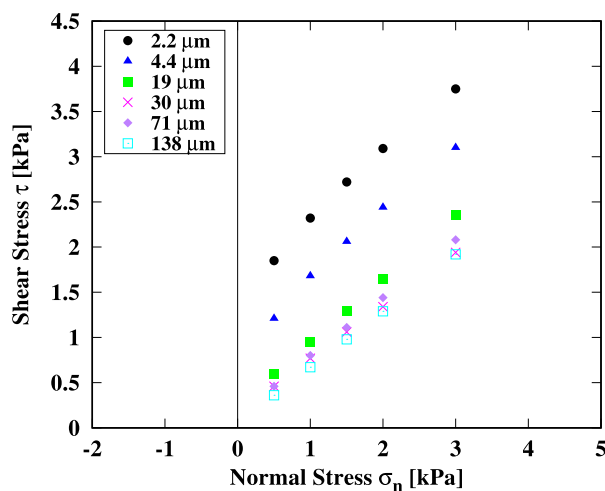


Fig. 6. Yield locus of different size limestone powders using the RST-01: shear stress  $\tau$ , plotted against normal stress,  $\sigma_n$ . The pre-shear normal stress  $\sigma_{pre}$  is set to 5 kPa but not shown here. Different symbols represent limestone samples with different median particle size as explained in the legend and each point represents three measurements.

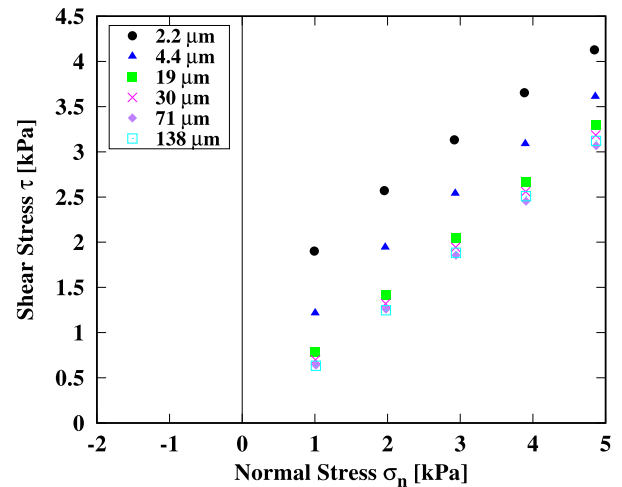


Fig. 7. Yield locus of different size limestone powders as in Fig. 6 using Brookfield PFT. The pre-shear normal stress  $\sigma_{pre} = 4.8$  kPa is not shown here.

them out when using the Brookfield powder flow tester. As expected, the size increase in powders leads to a lower resistance during shearing, thus a lower yield locus. The yield loci of 30, 71 and 138  $\mu\text{m}$  are almost collapsing on each other which was already reported in a previous study [24].

Although the semi-automated shear RST device is giving self-reproducible measurements, it is still worth to evaluate the raw yield loci data of PFT using the different size limestone powders also with the Brookfield PFT tester as shown in Fig. 7. The global trends of the yield loci measured by PFT is consistent with the trends from Fig. 6, which confirms the good qualitative agreement of both devices.

Furthermore, we have tested the two reference powders using both devices at the same pre-shear stress levels as shown in Fig. 8. The mean values are stable for both devices and all the standard deviations stay within the symbol size range (not shown) confirming self-repeatability. For the free flowing Eskal150, the yield loci demonstrate a very good agreement and the fitted curve matches all the data points. For the cohesive Eskal300, data from the

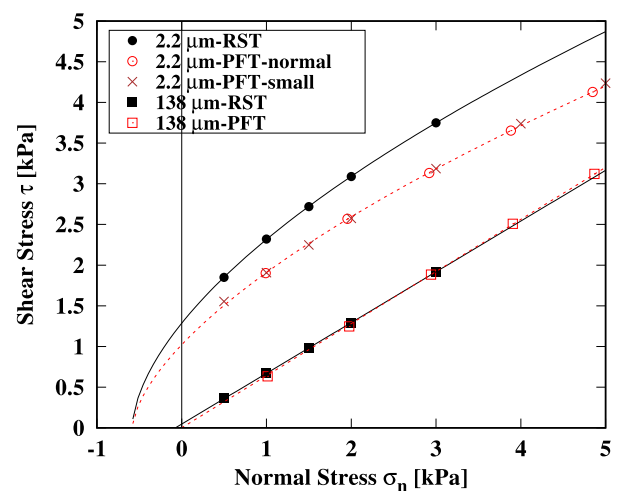


Fig. 8. Yield locus of two reference limestone powders: Eskal150 (138  $\mu\text{m}$ ) and Eskal300 (2.2  $\mu\text{m}$ ) using both RST-01 and Brookfield PFT. The pre-shear normal stresses  $\sigma_{pre}$  are set to 5 kPa for both devices. The nonlinear lines (2.2  $\mu\text{m}$ ) are the fitting to the raw data using Warren-Spring model with  $C = 1.29$  kPa,  $T = 0.58$  kPa,  $n = 1.69$  for RST and  $C = 1.02$  kPa,  $T = 0.58$  kPa,  $n = 1.60$  for PFT.

PFT are lower than that from the RST-01, but with similar non-linear curvature.

We can speculate about two reasons for the differences in the values we obtain for the shear stress with the Eskal300. The first one would be that the powders measured with the RST could be slightly more wet. This would increase the stickiness due to capillary forces. Therefore the yield locus would be higher [69].

The samples used were collected directly from original sealed bags, eliminating the possibility of being affected by humidity in such a short time. The reason for this difference would be in the geometry of the cells as explained by Schmitt and Feise (2004) [70]. In a later study, Berry (2007) [71] also reported that the value of the unconfined failure stress  $\sigma_c$  is strongly affected by the test protocol and the procedure of calculation used. Tim Bell (2012) also presented work for BCR-116 limestone and  $\text{TiO}_2$  on this issue and observed a difference in the geometry of the cells especially the narrow edge and curved (dome-like) cross-section of the PFT lid versus the Schulze tester. Although it was difficult to attribute the discrepancies to the lid geometry only since he also found differences in the software analysis of the yield locus and steady-state shear [72].

Regarding the protocol, the Brookfield tester measures the steady state shear after several (normally above 5) pre-shears but the Schulze ring shear tester determines that in one or two pre-shears. This could result in a slightly different pre-shear history, the more pre-shear cycles, the weaker the sample is expected to be. It is worth noting that the bed heights for the Brookfield tester and for the Schulze tester differed (15 mm and 24 mm, respectively). The distribution of the applied normal force through the sample, and therefore at the shear plane, could also potentially impact the results.

Berry [40] reported disparity between the Schulze ring shear tester and the PFT in his round robin study with CRM-116 limestone powder. These differences are usually attributed to the shear cell geometry (as mentioned above the annular lids of the two cells are different). The Schulze has open pockets (flat lid with vertical vanes) whilst the Brookfield PFT uses closed pockets. Schmitt and Feise [70] found that the standard Peschl cell which featured a flat lid with a knurled contact surface “to grip the powder” measured lower shear stresses than the same lid when fitted with “open pocket” vanes of the same dimensions used on the Schulze RST lid.

## 5.2. Non-linearity of Yield Locus at low pre-shear stress levels

The median particle size of powders affects cohesion that will influence the non-linearity of the yield locus as well as the powder flow behaviour. The smaller the particle size, the more cohesive the sample, therefore finer powders typically show higher yield stress and higher non-linearity. However, the role of the pre-shear stress is still unclear.

In Fig. 9, we look at the raw shear failure points of free-flowing Eskal150 (138  $\mu\text{m}$ ) at different pre-shear stress levels between 0.2 and 4 kPa. For all the pre-shear stress levels, all the shear failure points collapse on a linear curve, only few points at 3 kPa are deviating slightly from the curve, but within the standard deviation range. This indicates that the free-flowing powder is insensitive to the pre-shear stress change, and thus has both cohesion and tensile strength near zero.

However, when we look at the shear failure points of cohesive powders at different pre-shear stress levels as shown in Fig. 10, the shear failure points are separate from each other. With increasing the pre-shear stress levels, the failure shear stresses also increase, like cohesion and tensile strength, which is due to the pre-consolidation applied. Unlike the free-flowing powder, whose bulk density is not sensitive to the pre stress in this change. For the cohesive limestone powder the pre-shear stress leads to con-

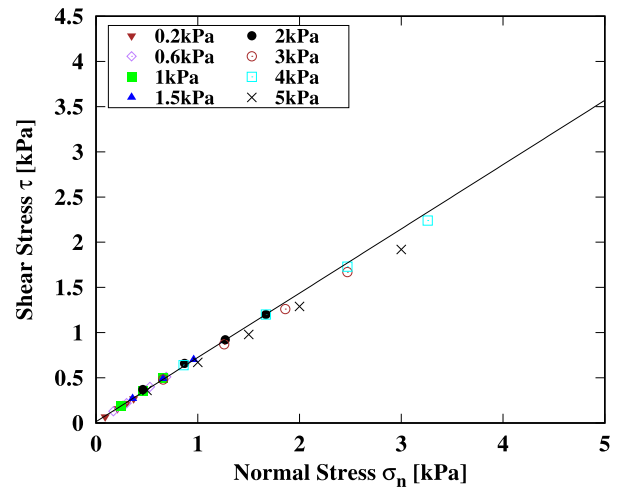


Fig. 9. Shear failure points of Eskal150 (138  $\mu\text{m}$ ) at pre-shear stress levels up to 5 kPa using RST-01. The line is the linear regression fitting to the raw data and pre-shear points are not shown here.

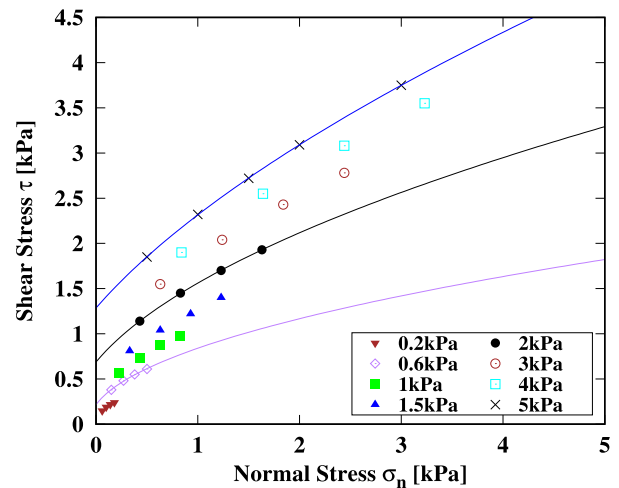


Fig. 10. Shear failure points of Eskal300 (2.2  $\mu\text{m}$ ) at pre-shear stress levels up to 5 kPa using RST-01. Lines are the fitting using the Warren-Spring model as shown in Eq. (2) with only 0.6, 2 and 5 kPa for the sake of clarity. The pre-shear points are also not shown here.

siderable compaction and thus the bulk density increases to form a stronger bulk solid.

After confirming the repeatability and reproducibility of our raw data from both Schulze RST-01 and Brookfield PFT, we fitted the Warren-Spring model on the raw yield loci of cohesive Eskal300 at different pre-shear stress levels.

The first important parameter is cohesion,  $C$ , which is the intercept of fitted non-linear yield locus to the  $\tau$ -axis. In Fig. 11, we plot the cohesion against the pre-consolidation normal stress for cohesive Eskal300 using both RST-01 and PFT. For RST-01, with increasing the pre-shear stress from 0.2 kPa to 35 kPa, the cohesion increases from 0.06 kPa to 3.31 kPa. While for PFT, we only tested a narrower range of pre-shear stress from 1 kPa to 4.8 kPa, due to the device limit on the high stress levels when using the normal cell. The cohesion increases from 0.31 kPa to 1.02 kPa. The cohesion values from PFT scatter to slightly lower values than the ones obtained from RST-01, but the trend of cohesion agrees very well between the two devices.

The values obtained using the Ajax tensile tester expressed in Pa for Eskal300 are given in Table 4. Note that the standard

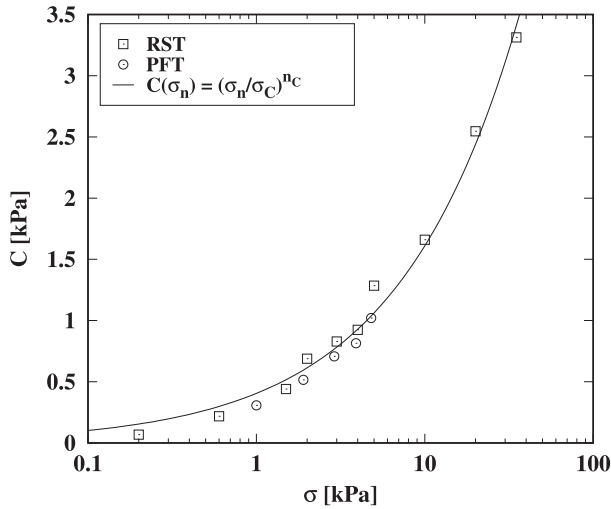


**Fig. 11.** Unconfined cohesion,  $C$ , plotted against pre-consolidation normal stress  $\sigma$  for cohesive Eskal300 (2.2  $\mu\text{m}$ ) using RST-01 and Brookfield PFT. The line is the fit to both RST and PFT data with the cohesive characteristic consolidation  $\sigma_c = 4.52$  kPa, and the slope  $n_c = 0.60$ .

**Table 4**  
Values obtained for the tensile strength using the Ajax Tester.

Consolidation	1.1 kPa	3 kPa	9 kPa	27 kPa
Average	131.3	262.5	619.8	1380.6
Standard deviation	61.7	58.3	64.7	89.1

deviation fluctuates since it is not easy to determine the point of fracture of the bed.

The second parameter in the model is the tensile strength,  $T$ , which is the intercept of the fitted non-linear yield locus to the  $\sigma_n$ -axis. The tensile strength normally comes in negative sign, which indicates the direction difference to the compressive stresses, e.g. pre-consolidation normal stress. For the sake of convenience, we present  $T$  in positive sign as shown in Fig. 12 for the same data as in Fig. 11. Similar to cohesion, the tensile strength increases from 0.01 to 1.70 kPa for RST-01 and from 0.12 to

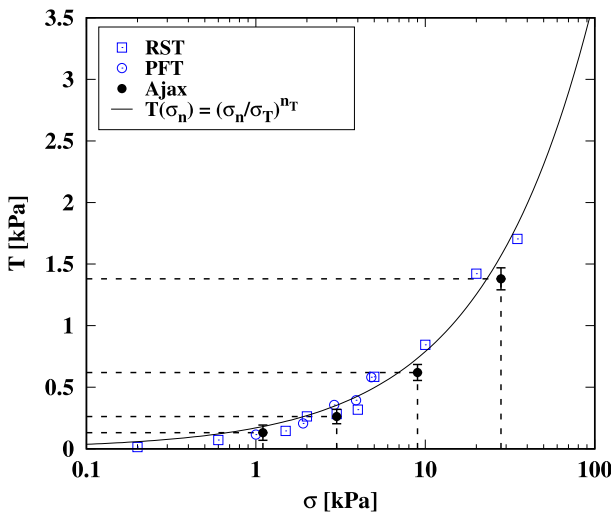


**Fig. 12.** Tensile strength,  $T$ , plotted against pre-consolidation normal stress  $\sigma$  for cohesive Eskal300 (2.2  $\mu\text{m}$ ) using RST-01, PFT and Ajax tensile tester with the tensile characteristic consolidation  $\sigma_T = 14.26$  kPa, and the slope  $n_T = 0.67$ .

0.58 kPa for PFT with increasing the pre-shear stress. The relative change of  $T$  is thus larger than that of  $C$ , almost in proportion to the variation of  $\sigma_n$ . The values from the two shear devices agree quite well, with similar scatter as  $C$ -data. On the same figure, we have also added the tensile strength directly measured from the Ajax tensile tester for different levels of consolidation (1.1, 3, 9 and 27 kPa). The results are based on appearance of a crack that builds up and propagates through the sample and there is plausible agreement with the results from the shear testers and validates the values obtained from Warren Spring model by non-linear extrapolation to negative stresses.

The last, but also the most interesting parameter in the model is the shear index,  $n$ , which indicates the degree of non-linearity of the yield locus. In Fig. 13, the shear index is plotted against the pre-consolidation stress the same data as Figs. 11 and 12. In contrast to cohesion and tensile strength, the shear index decreases from 2.05 to 1.41 for RST-01 and from 1.95 to 1.61 for PFT, with increasing pre-shear stress. This means lower pre-shear stress leads to higher non-linearity of the yield locus of Eskal300. In other words, with increasing in pre-shear stress, the yield locus becomes more linear but is still far from  $n = 1$  in the stress range tested here. In addition, the shear index seems to saturate around 2 when  $\sigma_n$  tends to zero and around value 1.4 at the high end ( $> 20$  kPa). This might be related to possible lowest/highest bulk density for cohesive powder, where the bulk density determines the non-linearity of the yield loci. Applying a compressive stress to a loose powder is expected to result in a decrease in the void fraction of the powder. Thus in Fig. 14 an increase in the preshear normal stress produces an increase in bulk density. In this plot values for RST and PFT agree quite well.

The behaviour of powders subjected to shear at different consolidation stresses can be characterized using the extrapolated values of the tensile strength  $T$  to normalize the stress relative to the maximal tensile strength (Fig. 15). The powder with smallest median particle size and strongest interparticle forces appears top left in the diagram (2.2  $\mu\text{m}$ ) and the other powders are placed lower and further right with increasing median particle size and normal stress. The descending trend offers a distinctive option for the classification of flowability from very poor (2.2  $\mu\text{m}$ ) to easy flowing (138  $\mu\text{m}$ ).

We can now define the Warren-Spring dimensionless number  $WS$  in Eq. (4) as the ratio of the (effective) compression-to-

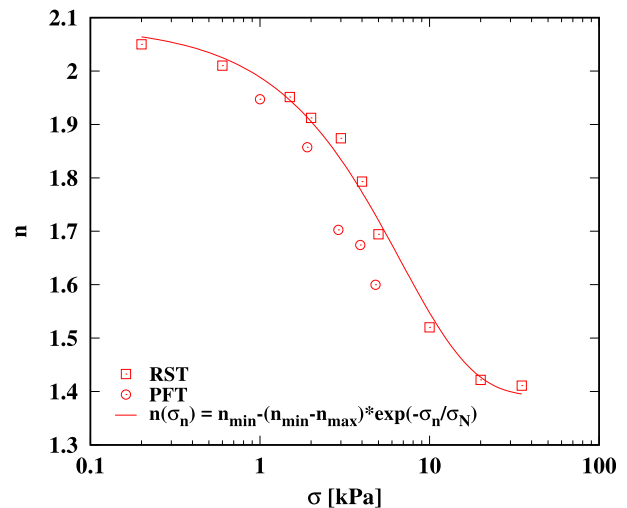


**Fig. 13.** Shear index,  $n$ , plotted against pre-consolidation normal stress  $\sigma$  for cohesive Eskal300 (2.2  $\mu\text{m}$ ) using RST-01 and PFT. The line is the fit to only RST data with  $\sigma_N = 7.02$  kPa,  $n_{min} = 1.41$  and  $n_{max} = 2.05$ .

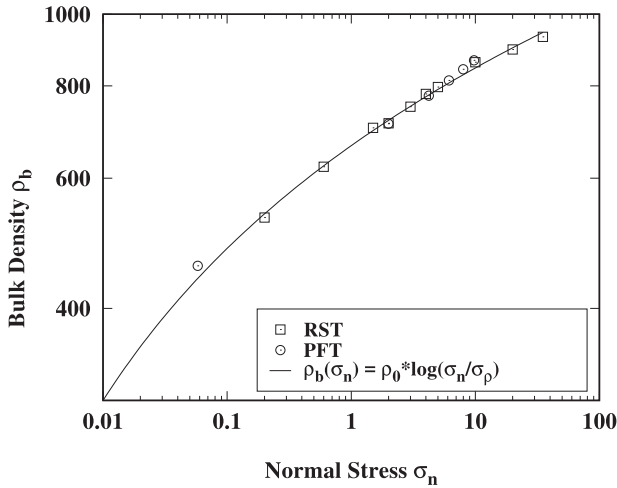


**Fig. 14.** Steady state bulk density  $\rho_b$  plotted against preshear normal stress  $\sigma_n$  for Eskal300 including both RST-01 and PFT. The line is the fit to the data up to 10 kPa pre-shear stress with  $\rho_0 = 79 \text{ kg/m}^3$  and  $\sigma_\rho = 0.0002 \text{ kPa}$ .

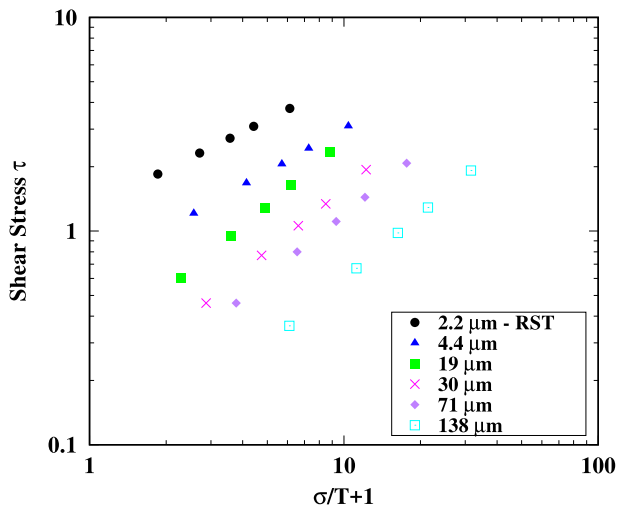


**Fig. 15.** Shear Stress  $\tau$  plotted against the ratio between normal stress and tensile strength  $\sigma/T + 1$  for different size limestone powders including only RST-01.

tension stress difference scaled which has been made dimensionless by the tensile strength.

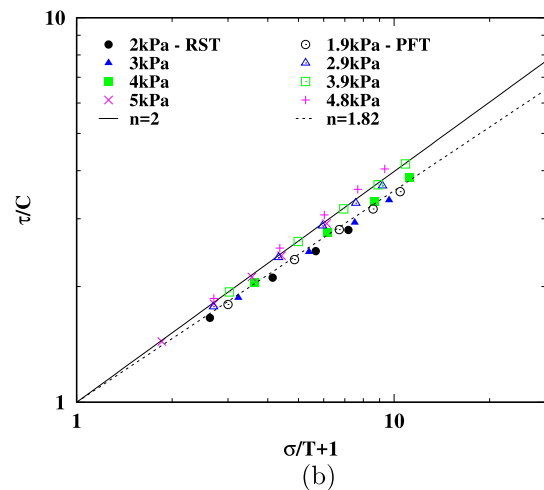
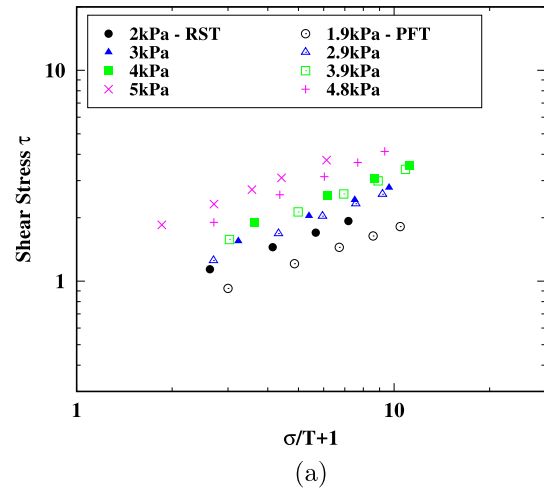
$$WS = \frac{\sigma_n + T}{T} \quad (4)$$

Fig. 16(a) depicts the influence of the pre-shear stresses in this classification plot for the most cohesive powder Eskal300 (2.2  $\mu\text{m}$ ) obtained by both RST and PFT, with their slightly different results. When the shear stress is normalized by cohesion, C, as shown in Fig. 16(b), the relationship deduced from the Warren-Spring model in Eq. (2), namely:

$$\left(\frac{\tau}{C}\right)^n = \frac{\sigma_n}{T} + 1 \quad (5)$$

is confirmed by the good data-collapse. The evident difference is the dimensionless shear index, n, with value 2 for RST and 1.82 for PFT, indicating that n is sensitive to the device and/or the procedure used.

A failure surface of Eskal300 superimposed involving the consolidation stress  $\sigma_n$ , the void fraction and the shear stress  $\tau$ , similar to the Hvorslev surface [73] is depicted in Fig. 17. This typical 3D



**Fig. 16.** (a) Shear stress,  $\tau$ , (b) shear stress normalized by cohesion,  $\tau/C$ , plotted against the ratio between normal stress and tensile strength  $\sigma/T + 1$  for Eskal300 at different preshear stresses including both RST-01 and PFT.

diagram is a graphical representation of the failure criteria including a family of curves for over consolidated states showing the mechanical properties of Eskal300.

The plot includes the critical state line and its projection considering the values of shear stress and the consolidation line when a powder is sheared in a shear cell under different normal stresses that lead to different void fractions. Failure is characterized by a critical value of void fraction. Consideration of different case studies shows that powder flow through a given process hardware remains the biggest uncertainty with respect to unexpected flow problems with single components or new formulations. Knowing this surface for a certain powder can tell us if it will flow. Between cohesive materials that suffer flow issues, the biggest parametric change is tensile strength. The line showing the variation of tensile strength at different packing densities of the bulk powders which affects the number and strength of particle contacts is also depicted in Fig. 17. This can be linked to inter-particle forces by a Rumpf-type approach, however, the effect of consolidation stress is critical.

The full function which could describe the Hvorslev surface with the analytical expressions and approximate coefficients taken from the data, see Figs. 11–14.

$$\tau(\sigma_n, \epsilon) = C(\sigma) * \left(\frac{\sigma_n}{T(\sigma)} + 1\right)^{1/n(\sigma)} \quad (6)$$

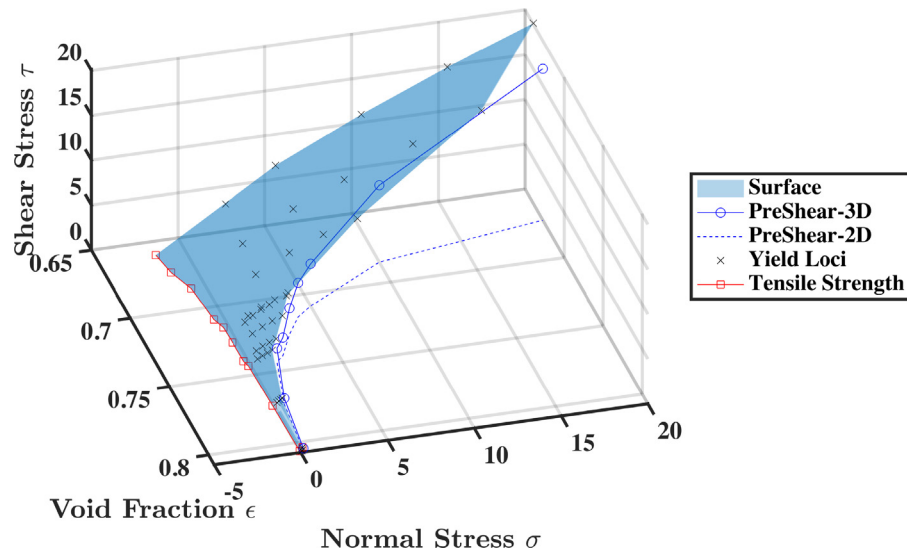


Fig. 17. Hvorslev diagram of the Eskal300 data measured using RST-01 at different preshear stresses.

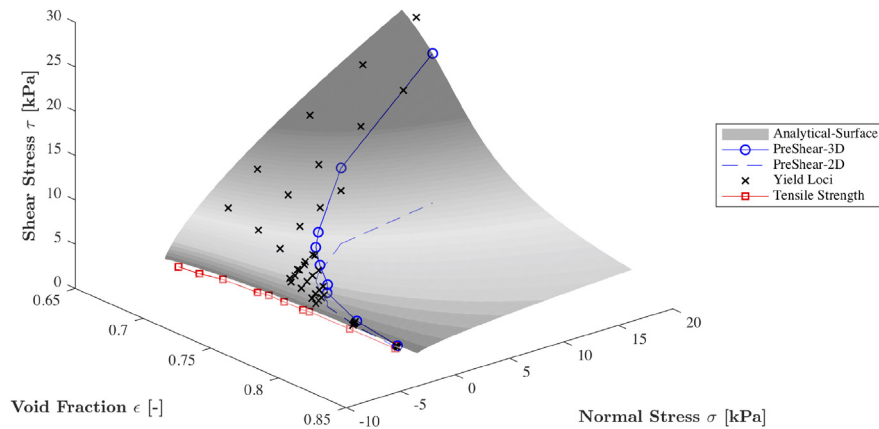


Fig. 18. The Eskal300 data measured using RST-01 at different preshear stresses and the analytical prediction of the Hvorslev surface using Eq. (6).

with  $C(\sigma) = (\sigma/4.6)^{0.6}$ ,  $T(\sigma) = (\sigma/14)^{0.67}$ ,  $n(\sigma) = 1.4 + 0.7 * \exp(-\sigma/6.7)$  and  $\sigma(\epsilon) = 1/2200 * \exp(1/(35\epsilon))$ .

The surface obtained using the analytical solution described in Eq. (6) is shown in Fig. 18 as well as a family of curves for over consolidated states and tensile strength values for Eskal300.

## 6. Conclusions

This study focuses on the tensile strength of cohesive particulate solids, where we use a range of limestone fractions of varying size and thus cohesion and tensile strength. All powders used in this study are dry (mostly insensitive to humidity); their properties are analysed by means of two shear testers, the Schulze Ring Shear tester and the Brookfield Powder Flow Tester. In particular, the sample Eskal300, with  $d_{50} = 2.2 \mu\text{m}$ , is used as the reference cohesive fine powder and stretched for detailed measurements. The shear testers are operated in the region of reduced stresses, with special focus on values under 5 kPa, and to complement these data the Eskal300 is also analysed by directly measuring the tensile strength with the Ajax tensile tester.

Analysing the results, we observe that the Warren-Spring model is a very good description and allows to extract the unconfined

cohesion,  $C$ , the extrapolated tensile strength,  $T$ , and the shear index,  $n$ , which characterizes the non-linearity of cohesive powder yield loci. These characteristic quantities depend strongly on the inter-particle forces as established during pre-shearing and pre-consolidation.

Comparing the results from different shear testers, we find overall very good qualitative agreement with small quantitative differences, since both testers follow similar procedures with regards to sample preparation and differ slightly with respect to measurement protocol and geometry. These differences are fortunately not leading to a great deviation in terms of tensile strength,  $T$ , although further experiments with a variety of cohesive powders are needed to confirm or rebut this point.

As major contribution, for the first time to our knowledge, the tensile strength,  $T$ , which must be extrapolated from shear tester data, was measured directly for the same fine, cohesive sample, Eskal300, for different consolidation stress levels (1.1, 3, 9 and 27 kPa), using the Ajax tensile tester. The tedious direct measurements match very well (within 10% margin) with the results from the shear testers, confirming that the non-linear extrapolation using the Warren-Spring model is valid and that the tensile strength is thus correlated closely to the cohesion of this powder. This observation requires further confirmation for many more powders.

From our results, for one powder so far, we conclude that the standard shear testers can very well be used to predict (by non-linear extrapolation, using the proper model) the tensile strength in the negative stress range. This is also supported by the perfect data-collapse we observe when plotting them against the “dimensionless effective tensile strength”,  $\sigma_n/T + 1$ , for a wide range of data, confirming that the Warren-Spring dimensionless number: WS, is nicely combining the interplay between tensile strength and confining stress.

The data necessary to analyse and interpret the effect of pre-consolidation and pre-shear of a powder on its mechanical properties based on the expansion failure, void fraction and the consolidation failure could be displayed in a 3-D diagram. A fashion model of the so-called Hvorslev surface is being actively developed based on the values obtained from the Warren Spring model, considering several yield loci at different consolidation stress levels.

The effect of particle size, shape, bulk density and surface energy on all the key model parameters is the ideal outcome of our investigations, which can then be used in the prediction of failure of single powder systems and formulations, or for continuum mechanical modeling of flow.

Such a model with predictive capability to directly quantify the response of powders to external stresses is a particularly valuable since it can directly impact manufacturing performance and efficiency.

#### Declaration of Competing Interest

The authors declare that there is no conflict of interest.

#### Acknowledgements

This collaborative paper has received funding from the Erasmus + training exchange scheme and the 4TU.Federation. This work was also supported by the European Union FP7 Marie Curie Actions Initial Training Network T-MAPPP (Training in Multiscale Analysis of MultiPhase Particulate Processes and Systems) under grant agreement No. 607453.

The authors would also like to thank Mr. Vivek Garg, Dr. Rob Berry and Prof. Mike Bradley (Wolfson Centre for Bulk Solids Handling Technology, University of Greenwich, UK) for the procurement of the samples and their valuable assistance in dealing with experimental and theoretical questions; as well as Dr. Ramon Cabiscol (TU Braunschweig, Germany) for the help on the material characterizations.

We also thank Ajax Equipment Ltd for making available the tensile tester instrument for these experiments, as well as the technical support and fine-tuning from Mr. Simon Fields.

#### References

- [1] A.J. Liu, S.R. Nagel, Nonlinear dynamics: Jamming is not just cool any more, *Nature* 396 (1998) 21–22.
- [2] D. Bi, J. Zhang, B. Chakraborty, R.P. Behringer, Jamming by shear, *Nature* 480 (2011) 355–358.
- [3] S. Luding, Granular matter: so much for the jamming point, *Nature* 12 (2016) 531–532.
- [4] N. Kumar, S. Luding, Memory of jamming–multiscale models for soft and granular matter, *Granular Matter* 18 (2016) 1–21.
- [5] M.E. Cates, M.D. Haw, C.B. Holmes, Dilatancy, jamming, and the physics of granulation, *J. Phys.: Condens. Matter* 17 (24) (2005) S2517–S2531, <https://doi.org/10.1088/0953-8984/17/24/010>.
- [6] M. Van Hecke, Jamming of soft particles: geometry, mechanics, scaling and isostaticity, *J. Phys.: Condens. Matter* 22 (2009) 033101.
- [7] Y. Yang, W. Fei, H.-S. Yu, J. Ooi, M. Rotter, Experimental study of anisotropy and non-coaxiality of granular solids, *Granular Matter* 17 (2015) 189–196.
- [8] K.A. Alshibli, S. Sture, Shear band formation in plane strain experiments of sand, *J. Geotech. Geoenviron. Eng.* 126 (2000) 495–503.
- [9] A. Singh, V. Magnanimo, K. Saitoh, S. Luding, Effect of cohesion on shear banding in quasistatic granular materials, *Phys. Rev. E* 90 (2014) 022202+.
- [10] S.C. Thakur, H. Ahmadian, J. Sun, J.Y. Ooi, An experimental and numerical study of packing, compression, and caking behaviour of detergent powders, *Particulate* 12 (2014) 2–12.
- [11] F. Radjai, M. Jean, J.J. Moreau, S. Roux, Force distribution in dense two-dimensional granular systems, *Phys. Rev. Lett.* 77 (1996) 274.
- [12] S. Luding, Anisotropy in cohesive, frictional granular media, *J. Phys. Condens. Matter* 17 (2005).
- [13] T.S. Majmudar, R.P. Behringer, Contact force measurements and stress-induced anisotropy in granular materials, *Nature* 435 (2005) 1079–1082.
- [14] S.B. Savage, K. Hutter, The motion of a finite mass of granular material down a rough incline, *J. Fluid Mech.* 199 (1989) 177.
- [15] P.A. Cundall, Numerical experiments on localization in frictional materials, *Ingenieur-Archiv* 59 (1989) 148–159.
- [16] F. Radjai, S. Roux, J.J. Moreau, Contact forces in a granular packing, *Chaos* 9 (1999) 544–550.
- [17] B. Wolf, R. Scirocco, W.J. Frith, I.T. Norton, Shear-induced anisotropic microstructure in phase-separated biopolymer mixtures, *Food Hydrocolloids* 14 (2000) 217–225.
- [18] G.D.R. Midi, On dense granular flows, *Eur. Phys. J. E* 14 (2004) 341–365.
- [19] J. Tomas, Product design of cohesive powders – mechanical properties, compression and flow behavior, *Chem. Eng. Technol.* 27 (2004).
- [20] F. Alonso-Marroquin, H.J. Herrmann, Ratcheting of granular materials, *Phys. Rev. Lett.* 92 (2004) 54301.
- [21] S. Luding, Shear flow modeling of cohesive and frictional fine powder, *Powder Technol.* 158 (2005) 45–50.
- [22] S. Luding, Cohesive, frictional powders: contact models for tension, *Granul. Matter* 10 (2008) 235–246.
- [23] M. Morgeneyer, L. Brendel, Z. Farkas, D. Kadav, D.E. Wolf, J. Schwedes, Can one make a powder forget its history?, in: *Proceedings of the 4th International Conference for Conveying and Handling of Particulate Solids, Budapest, 2003*, pp. 12–118.
- [24] H. Shi, R. Mohanty, S. Chakravarty, R. Cabiscol, M. Morgeneyer, H. Zetzener, J.Y. Ooi, A. Kwade, S. Luding, V. Magnanimo, Effect of particle size and cohesion on powder yielding and flow, *KONA Powder Particle J.* 35 (2018) 226–250.
- [25] J. Schwedes, Review on testers for measuring flow properties of bulk solids, *Granul. Matter* 5 (2003) 1–43.
- [26] A.W. Jenike, Quantitative design of mass-flow bins, *Powder Technol.* 1 (1967) 237–244.
- [27] J. Schwedes, D. Schulze, Measurement of flow properties of bulk solids, *Powder Technol.* 61 (1) (1990) 59–68, [https://doi.org/10.1016/0032-5910\(90\)80066-8](https://doi.org/10.1016/0032-5910(90)80066-8).
- [28] D. Schulze, Time- and velocity-dependent properties of powders effecting slip-stick oscillations, *Chem. Eng. Technol.* 26 (2003) 1047–1051.
- [29] G. Mehos, J. Carson, Bulk Solids Flow and Hopper Design, Subsection in *Perry's Chemical Engineers Handbook*, ninth ed., McGraw-Hill, 2018.
- [30] A. Russell, P. Müller, H. Shi, J. Tomas, Influences of loading rate and preloading on the mechanical properties of dry elasto-plastic granules under compression, *AIChE J.* 60 (2014) 4037–4050.
- [31] O.I. Imole, M. Paulick, V. Magnanimo, M. Morgeneyer, B.E. Montes, M. Ramaioi, A. Kwade, S. Luding, Slow stress relaxation behavior of cohesive powders, *Powder Technol.* 293 (2016) 82–93.
- [32] M. Morgeneyer, J. Schwedes, Investigation of powder properties using alternating strain paths, *Task Quart.* 7 (2003) 571–578.
- [33] H. Feise, J. Schwedes, Investigation of the behaviour of cohesive powder in the biaxial tester, *Kona Powder Part. J.* 13 (1995) 99–104.
- [34] A. Casagrande, The determination of the pre-consolidation load and its practical significance, *Proceedings of the International Conference on Soil Mechanics and Foundation Engineering*, vol. 3, Harvard University, Cambridge, 1936, pp. 60–64.
- [35] J. Schwedes, Vergleichende betrachtungen zum einsatz von schergeräten zur messung von schüttguteigenschaften, in: *Proc. PARTEC, Nürnberg, 1979*, pp. 278–300.
- [36] S. Shibuya, T. Mitachi, S. Tamate, Interpretation of direct shear box testing of sands as quasi-simple shear, *Geotechnique* 47 (1997) 769–790.
- [37] A.W. Jenike, Storage and Flow of Solids, Bulletin no. 123, Bulletin of the University of Utah 53, 1964.
- [38] R. Freeman, Measuring the flow properties of consolidated, conditioned and aerated powders – a comparative study using a powder rheometer and a rotational shear cell, *Powder Technol.* 174 (2007) 25–33.
- [39] D. Schulze, Entwicklung und Anwendung eines neuartigen Ringschergerätes, *Aufbereitungs-Technik* 35 (1994) 524–535.
- [40] R.J. Berry, M.S.A. Bradley, R.G. McGregor, Brookfield powder flow tester—results of round robin tests with CRM-116 limestone powder, *Proc. Inst. Mech. Eng. Part E: J. Process Mech. Eng.* 229 (2015) 215–230.
- [41] H. Tsunakawa, R. Aoki, Measurements of the failure properties of granular materials and cohesive powders, *Powder Technol.* 33 (1982) 249–256.
- [42] D. Schulze, *Powders and Bulk Solids: Behavior, Characterization, Storage and Flow*, Springer, 2008.
- [43] J. Harder, J. Schwedes, The development of a true biaxial shear tester, *Part. Part. Syst. Char.* 2 (1985) 149–153.
- [44] R.J.M. Janssen, H. Zetzener, Measurements on cohesive powder with two biaxial shear testers, *Chem. Eng. Technol.* 26 (2003) 147–151.
- [45] J.P. Bardet, *Experimental Soil Mechanics*, Prentice-Hall, Upper Saddle River, New Jersey, 1997.
- [46] M.D. Ashton, D.C.H. Cheng, R. Farley, F.H.H. Valentin, Some investigations into the strength and flow properties of powders, *Rheol. Acta* 4 (1965) 206–218.

- [47] D.-H. Cheng, The tensile strength of powders, *Chem. Eng. Sci.* 23 (1968) 1405–1420.
- [48] P. Hartley, G. Parfitt, An improved split-cell apparatus for the measurement of tensile strength of powders, *J. Phys. E: Sci. Instrum.* 17 (1984) 347.
- [49] H. Rumpf, "The strength of granules and agglomerates" in *Agglomeration*, in: W.A. Knepper (Ed.), *Agglomeration*, Proc. 1st International Symposium on Agglomeration, Philadelphia, PA, John Wiley & Sons, New York, 1962, pp. 379–418.
- [50] M. Capece, R. Ho, J. Strong, P. Gao, Prediction of powder flow performance using a multi-component granular bond number, *Powder Technol.* 286 (2015) 561–571.
- [51] V. Garg, S. Mallick, P. Garcia-Trinanes, R.J. Berry, An investigation into the flowability of fine powders used in pharmaceutical industries, *Powder Technol.* 336 (2018) 375–382.
- [52] D. Schulze, Round robin test on ring shear testers, *Adv. Powder Technol.* 22 (2011) 197–202.
- [53] S. Kamath, V.M. Puri, H.B. Manbeck, R. Hogg, Flow properties of powders using four testers—measurement, comparison and assessment, *Powder Technol.* 76 (1993) 277–289.
- [54] S. Kamath, V.M. Puri, H.B. Manbeck, Flow property measurement using the Jenike cell for wheat flour at various moisture contents and consolidation times, *Powder Technol.* 81 (1994) 293–297.
- [55] R.J. Akers, The certification of a limestone powder for jenike shear testing (CRM 116), EUR (Luxembourg), 1992.
- [56] S. Koynov, B. Glasser, F. Muzzio, Comparison of three rotational shear cell testers: powder flowability and bulk density, *Powder Technol.* 283 (2015) 103–112.
- [57] L. Parrella, D. Barletta, R. Boerefijn, M. Poletto, Comparison between a uniaxial compaction tester and a shear tester for the characterization of powder flowability, *KONA Powder Particle J.* 26 (2008) 178–189.
- [58] H. Salehi, D. Barletta, M. Poletto, A comparison between powder flow property testers, *Particuology* 32 (2017) 10–20.
- [59] E. Teunou, J.J. Fitzpatrick, E.C. Synnott, Characterisation of food powder flowability, *J. Food Eng.* 39 (1999) 31–37.
- [60] J.J. Fitzpatrick, S.A. Barringer, T. Iqbal, Flow property measurement of food powders and sensitivity of Jenike's hopper design methodology to the measured values, *J. Food Eng.* 61 (2004) 399–405.
- [61] H.J. Feise, A review of induced anisotropy and steady-state flow in powders, *Powder Technol.* 98 (1998) 191–200.
- [62] H. Zetzener, J. Schwedes, Relaxation and creep of dry bulk solids, *Part. Part. Syst. Charact.* 19 (2002) 144–148.
- [63] D. Schulze, Towards more reliability in powder testing (v), in: *Proceedings of the 4th International Conference for Conveying and Handling of Particulate Solids (CHoPS)*, Budapest, 2003, pp. 5–31.
- [64] A. D6773-16, Standard Shear Test Method for Bulk Solids using The Schulze Ring Shear Tester, West ASTM International, Conshohocken, PA, 2008.
- [65] P. Stainforth, R. Berry, A general flowability index for powders, *Powder Technol.* 8 (1973) 243–251.
- [66] M. Peleg, M.D. Normand, Cohesion and tensile strength estimation from incomplete shear analysis data, *Powder Technol.* 326 (2018) 288–291.
- [67] M. Hirota, K. Takenaka, K. Iimura, M. Suzuki, Proposal of an approximation equation for the yield locus to evaluate powder properties, *Adv. Powder Technol.* 18 (2007) 287–302.
- [68] Y. Shimada, S. Hatano, S. Matsusaka, A new method for evaluating powder flowability using constant-volume shear tester, *Adv. Powder Technol.* 29 (2018) 3577–3583.
- [69] P. Pierrat, D.K. Agrawal, H.S. Caram, Effect of moisture on the yield locus of granular materials: theory of shift, *Powder Technol.* 99 (1998) 220–227.
- [70] R. Schmitt, H. Feise, Influence of tester geometry, speed and procedure on the results from a ring shear tester, *Part. Part. Syst. Charact.* 21 (2004) 403–410.
- [71] R. Berry, M. Bradley, Investigation of the effect of test procedure factors on the failure loci and derived failure functions obtained from annular shear cells, *Powder Technol.* 174 (2007) 60–63.
- [72] T. Bell, *Mechanics of particulate solids*, Annual Meeting of the EFCE Working Party, (2012) Friedrichshafen, Germany, 2012.
- [73] M.J. Hvorslev, Physical components of the shear strength of saturated clays., Technical Report, Army Engineer Waterways Experiment Station Vicksburg Ms, 1961.